The distribution of misorientations and grain boundary planes in grain boundary engineered brass

Valerie Randle*, Yan Hu*, Gregory S. Rohrer[+] and Chang-Soo Kim[+]

*Materials Research Centre, School of Engineering, University of Wales Swansea, Swansea SA2 8PP, UK.
[+]Department of Materials Science and Engineering, Carnegie Mellon University, Pittsburgh, PA 15213-3890, USA.

Abstract

In this paper we report the application of a five-parameter determination of grain boundary types to grain boundary engineered alpha-brass. The data are discussed particularly in terms of the distribution of boundary planes, and also with respect to the potential relationship between the planes distribution and the misorientation distribution. Approximately 20,000 grains comprised the total sample population, giving rise to more than 77,000 grain boundary line segments. This is the first time that the orientation of a large sample population of grain boundary planes has been measured in a grain boundary engineered material. The most important findings of the investigation were that the distribution of planes shows a prevalence of <110> tilt boundaries, especially asymmetric tilt types, and the presence of <111> twist boundaries. This distribution is a consequence of the low energy of these boundary types. Furthermore more than three-quarters of boundaries could be considered to be 'potentially special'. The presence of these boundaries greatly fragmented the grain boundary network. This fragmentation is probably a key factor in the development of superior properties in a grain boundary engineered material.

Introduction

'Grain boundary engineering' (GBE) is the manipulation of grain boundary structure in order to improve material properties. For example GBE has been known to mitigate intergranular stress corrosion cracking in nickel-based alloys.[1] Grain boundary engineering has recently been reviewed in detail.[2]

In low stacking-fault energy metals and alloys GBE is brought about by prolific annealing twinning. The annealing twin is characterised in the coincidence site lattice (CSL) notation as a particular type of $\Sigma 3$ having the interface plane either on {111} (the 'coherent twin') or {112} (the 'incoherent twin'). Boundary types in GBE materials are usually categorised based on misorientation alone, rather than on the indices of the boundary plane. Further progress in understanding the mechanisms of GBE requires a more in-depth knowledge of grain boundary structure, since 'special' boundaries in polycrystals are not identified by only the three misorientation parameters, but also by the two parameters that specify the orientation of the boundary plane.[3] Recently a method has been designed to measure all five grain boundary parameters. In the first instance the method required serial sectioning to obtain the inclination of boundary surfaces.[4] More recently a stereological method has been devised to extract data on all five grain boundary parameters from a single planar section through the specimen.[5]

In this paper we report the application of the five-parameter determination of grain boundary types to GBE alpha-brass. The data are discussed particularly in terms of the distribution of boundary planes, and also with respect to the potential relationship between the planes distribution and the misorientation distribution.

Experimental

Specimens of alpha-brass underwent GBE processing by five iterations of 25% uniaxial strain followed by annealing in air for 300s at 665°C. Full details of the processing, specimen preparation and effect on properties have been published elsewhere.[6] Many high resolution electron back-scatter diffraction (EBSD) orientation maps of the specimen were obtained using HKL Channel 5 software interfaced to a Philips XL30 scanning electron microscope operated at an accelerating voltage of 20kV. Maps were obtained by beam scanning followed by stitching together contiguous regions. A step size of 2μm was used for mapping. Approximately 20,000 grains comprised the total dataset. Calculations of symmetry-related misorientation solutions were performed using programs written in-house at Swansea.

The orientation data were used to determine the grain boundary character distribution, $f(\Delta g, n)$, which is defined as the relative areas of distinguishable grain boundaries characterized by their lattice misorientation (Δg) and boundary plane orientation (n).[7] The grain boundary character distribution is measured in multiples of a random distribution (MRD). Each grain boundary connecting two triple points can be broken up into to several line segments, referred to as grain boundary traces. The direction of the trace and the lattice misorientation across each trace specify four of the five parameters necessary to determine the distribution: the only unknown parameter is the inclination of the boundary plane with respect to the surface. If a sufficient number of grain boundary traces from randomly orientated, symmetrically indistinguishable bicrystals are observed, then stereology can be used to specify the probability that certain grain boundary planes appear in the microstructure.[5] In this case, our data set was made up of 77,000 grain boundary traces extracted from the orientation maps using a procedure described by Wright and Larsen.[8] The grain boundary character distribution, $f(\Delta g, n)$, is parameterized and discretized as described in our previous work, and therefore has a resolution of approximately 10 °.[4]

Results

Figure 1 is one of the orientation maps from GBE brass showing $\Sigma 3^n$ boundaries up to n = 5, i.e. $\Sigma 243$. $\Sigma 3$, $\Sigma 9$, $\Sigma 27$, $\Sigma 81$ and $\Sigma 243$ are coloured red, blue, yellow, green and purple respectively. Low angle boundaries (3º-15º) are grey and all remaining boundaries are black. More than half of the total boundary length in the map is $\Sigma 3$. Such prolific twinning resulted in the generation of higher order twins, particularly $\Sigma 9$ and $\Sigma 27$, but these boundaries tended not to survive in the microstructure other than as linkages between $\Sigma 3$s because interaction events with other $\Sigma 3^n$s regenerate $\Sigma 3$s, and hence there is only 3.4% $\Sigma 9$, 1.9% $\Sigma 27$, 1.1% $\Sigma 81$ and 0.1% $\Sigma 243$ by length.[9] There were no other CSLs present at levels above that expected for random generation. The orientation distribution (texture) is randomly distributed, which is a consequence of multiple twinning.

The grain boundary misorientation statistics derived from the orientation maps are given in Table 1. When the grain boundary statistics are calculated according to numbers of boundaries rather than as a fraction of grain boundary length, the proportion of $\Sigma 3$s drops drastically whereas the proportion of other boundaries increases. This is because of the dual effects of the morphology of annealing twins and that $\Sigma 3^n$s other than $\Sigma 3$s are present as many, usually short, bridging linkages.[2,9]

Following the five parameter analysis, the population densities of boundary plane normals are plotted in stereographic projection as multiples of a random distribution (MRD) for either the entire data set or subsets based on selected misorientations. The entire data set comprised approximately 77,000 line segments. It was found that the statistics generated by the {111} planes of the coherent twins dominated the distribution, which is not surprising because half the interface population is $\Sigma 3$. Therefore it was considered more insightful to examine that subset of the population which excludes $\Sigma 3$s. This subset of the population accounts for approximately 47,000 line segments, which is sufficient data to produce reliable grain boundary plane statistics.[5]

In order to discover trends in the five-parameter distribution, it was necessary to view the distribution of boundary planes according to misorientation subsets based on various misorientation axes, <100>, <110> and <111> were chosen because they are the lowest index misorientation axes and moreover Σ3, Σ9 and Σ27a will be included in these distributions because they have disorientations (i.e. lowest angle misorientations) of 60°/<111>, 39°/<110> and 32°/<110> respectively.

It was found that misorientations on <100> were very poorly represented, actually below that expected for a random distribution. On the other hand misorientations on <110> and <111> were present at levels well above those for a random distribution. Figure 2 shows the distribution of planes for the <110> misorientation axis, segmented into misorientation angle bins of 10°, from misorientation angles 10º to 60º. Σ3s have been excluded. Since the resolution of the plots is 10°, a small proportion of data from the 70°/<110> symmetry-related description of a Σ3 class can appear in the 60°/<110> category, which is probably responsible for the MRD = 4. The location of the misorientation axis, chosen to be [110], is marked on one of the plots. It is quite striking that for all misorientation angles the boundary planes lie preferentially on the zone of [110] (that is, they are tilt boundaries), with the maximum MRD in each plot ranging from nearly 4 to nearly 19. Although this trend is apparent in all the angle ranges, it is strongest in the 30° and 40° misorientation angle plots, which is where Σ27a and Σ9 resides. There is more than one maximum on each of the [110] zones, indicating that the tilt boundaries are asymmetric.

Figure 3 shows boundary planes for misorientations about <111> and misorientation angles 20º to 50º. As in Fig. 2, Σ3s have been excluded from the sample population because the peak for (111) planes at 60°/<111>, the coherent twin, is more than 2200 MRD, which overshadows the resolution in the other angle ranges. Figure 3 shows that for each misorientation angle class there is a single peak at (111) twist configuration with an MRD greater than 3.3.

As a consequence of the multiple twinning Σ27b, in addition to Σ27a, is present in the data at levels higher than expected for random generation. There are approximately equal numbers of Σ27a and Σ27b in the population, as shown in Table 1. Figure 4 shows the distribution of planes for Σ27b, where the disorientation is 35°/<210>, and it can be seen that there is a zone of planes which corresponds broadly to the <110> zone. The peaks on this zone are up to 4 MRD. The peaks are more diffuse than those for misorientations on <110> and <111> which were shown on Figs. 2 and 3.

Discussion

The five-parameter analysis has highlighted important trends in the data which are not revealed from an analysis of misorientation alone. The most striking points are the prevalence of <110> tilt boundaries, especially asymmetric tilt types, and the presence of <111> twist boundaries. Previous work has highlighted the importance of asymmetric boundaries, as opposed to symmetric types, in polycrystals.[10,11] From a probability point of view, there are many more possible asymmetric boundaries than symmetric ones, even when only tilt boundaries and low index planes are considered. For example, misorientations about <110> give rise to two symmetric boundaries on {111} and {112} (Σ3 coherent and incoherent twins respectively) and many asymmetric boundaries such as {411}{110}, {511}{111}, {221}{100}, {211}{552}, {221}{744} etc.[12] Geometrical constraints dictate that an asymmetrical boundary usually comprises only one low-index plane, because once the indices of the plane on one side of the boundary are selected, the indices of the second plane are fixed according to the misorientation. Figure 2 shows evidence that often one plane is near {111}. There is no evidence in Fig. 2 of a preference for the symmetrical planes of Σ9 and Σ27a, which are {411} and {221} in the case of Σ9 and {721} in the case of Σ27a, even though the 30º/<110> and 40º/<110> sections in Fig. 2 must include many Σ27a and Σ9 segments respectively.

A preference for asymmetrical tilt boundaries has been noted previously both from high resolution electron microscopy observations[10] and from EBSD-based measurements of boundary planes.[13] Based on previous work, which has shown an inverse relationship between the frequency with which boundaries

occur in the population and their energy, we assume that boundary types with high populations are also low energy boundaries.[4,14-16] This assumption is supported by the results of calculations which have shown that asymmetric boundaries may have low energies when bounded by low-index planes[17] and that <110> tilts in particular lie in an energy valley.[12] Therefore, in the present data, it is reasonable to conclude that <110> tilt and near tilt boundaries have low energies and that this is the reason for their prevalence.

The presence of quite high proportions of <111> twist boundaries is probably also associated with a low energy configuration, since the presence of two low index planes such as {111} at a grain boundary implies a lower than average energy, even when they mutually rotated.[16] It should be noted that, apart from the Σ3 misorientation, the population of low energy {111} twists does not correspond to CSL boundaries. Similarly, apart from Σ9 and Σ27a, the asymmetric tilts on <110> do not correspond to CSLs.

So far the data have been considered in terms of disorientation. For convenience, misorientation data are usually viewed from this standpoint. However, the disorientation may not contain the misorientation axis closest to a low-index axis.[18,19] For example whereas the disorientation for Σ27b is 35°/<210>, a symmetry-related solution for the Σ27b disorientation is 146º/<771>, and this axis is only 5.8º from 110. In Fig. 4 the planes distribution for Σ27b is interesting since it appears to lie on or near the <110> zone. This could be because there is a misorientation solution for Σ27b where the axis is close to <110>, giving rise to <110> tilt boundaries.

Other misorientations which are present in the sample population and whose disorientations are not on low index axes might also have a low index axis solution, similar to the case for Σ27b described above. To discover if this is the case, a scrutiny of all the symmetry-related solutions for misorientations on <110> and <111> was carried out. The motivation for this part of the study is that the data in Figs. 2 and 3 clearly show that misorientations on <110> and <111> are significant in terms of promoting low index boundary planes and are therefore important in the microstructure.

Table 2 shows the disorientation associated with misorientation angle/axis pairs on <110> in angle increments of 5° from 65° to 120°. Misorientations having angles $\theta \geq 120°$ are symmetry-related on <110> to solutions having (180° - θ) and therefore already appear as disorientations. Similarly solutions close to 70° misorientation angle, or equivalently close to 110°, are represented as disorientations close to 60°/<111>, i.e. Σ3. The remaining misorientations, 80°, 85° and 90°, are equivalently represented by disorientations approximating to 60°/<332>, 62°/<221> and 62°/<773> respectively. These disorientations can therefore also give rise to <110> asymmetrical tilt boundaries.

Turning to misorientations on <111>, those having angles >65° are all symmetry-related on <111> to disorientations. Hence all misorientations which are exactly on <111> are already represented by the disorientation solution. However, if the misorientation axis is slightly displaced from <111>, e.g. <776> (which is 4° from <111>), there are several disorientations which are equivalent to misorientations on <776>, i.e. close to <111>. These are 35°/<332>, 21°/<221>, 21°/<211>, 36°/<322> and 51°/<755>. To illustrate this point in Table 3 we show two examples, taken from the orientation map in Fig. 1.

A consequence of the exercise to search for all misorientations near <110> and <111> is that there are other disorientations which should be included in the statistics. Table 4 shows the proportions of the <110> and <111> misorientations (as a length fraction) for the orientation map in Figure 1, including those where the disorientation is not <110> or <111>. There may be other boundaries in the sample population which have a misorientation close to <110> or <111>, but these have not been assessed at this time and are likely to be small proportions. For non-CSL boundaries a tolerance of 7º on the misorientation axis and 5º on the misorientation angle was allowed. The Σ27b fraction, 0.9%, is included because it has a misorientation solution close to <110> and it is significant in the microstructure. Low angle boundaries are also included because it is known that they usually have 'special' (i.e. different from average) properties. Although 59.1% of boundary is on <111>, 57.7% of the total boundary length is accounted for as Σ3.

Figure 5a shows the same orientation map as in Fig. 1, with the boundaries listed in Table 4 coloured pale grey and the remaining boundaries black. These boundaries constitute three-quarters of the total boundary length, and could be considered to be 'potentially special', based on the evidence from the five-parameter analysis. It can be seen in Fig. 5a that the remaining network of random boundaries, coloured black, is very fragmented by the presence of the remaining grey boundaries. This fragmentation is probably a key factor in the development of superior properties in a grain boundary engineered material.

Conclusions

The distribution of grain boundary misorientations and planes has been acquired for more than 20,000 grains in grain boundary engineered brass. This is the first time that the orientation of a large sample population of grain boundary planes has been measured in a grain boundary engineered material. The most important findings of the investigation are:

- The distribution of planes shows a prevalence of <110> tilt boundaries, especially asymmetric tilt types, and the presence of <111> twist boundaries. This distribution is a consequence of the low energy of these types of boundary.
- More than three-quarters of boundaries could be considered to be 'potentially special'. The presence of these boundaries greatly fragmented the grain boundary network. This fragmentation is probably a key factor in the development of superior properties in a grain boundary engineered material.

References

1. P. LIN, G. PALUMBO, U. ERB, K. T. AUST: *Scripta Met. Mater*., 1995, 33, 1387-1392.
2. V. RANDLE: *Acta Mater*., 2004, 52, 4067-4081.
3. V. RANDLE: *Mater. Charact*., 2001, 47, 411-416.
4. D. M. SAYLOR, A. MORAWIEC AND G. S. ROHRER: *Acta Mater*. 2003, 51, 3663-3674.
5. D. M. SAYLOR, B. L. ADAMS, B. S. EL DASHER AND G.S. ROHRER: *Metall. Mater. Trans.*, 2003, 34A, 1-9.
6. V. RANDLE AND H. DAVIES: *Mater. Trans*., 2002, 33A, 1853-1857.
7. G. S. ROHRER, D. M. SAYLOR, B. S. EL-DASHER, B. L. ADAMS, A. D. ROLLETT AND P. WYNBLATT: *Z. Metall.* 2004, 95, 197-214
8. S. I. WRIGHT AND R. J. LARSEN: *J Micros*. 2002, 205, 245-
9. V. RANDLE: *Acta Mater*., 1999, 47, 4187-4196.
10. K. L. MERKLE: *Scripta Metall*., 1989, 23, 1487-1492.
11. K. L. MERKLE: *Ultramicroscopy*, 1991, 37, 130-
12. U. WOLF, F. ERNST, T. MUSCHIK, M. F. FINNIS AND H. F. FISCHMEISTER: *Philos. Mag.* 1992, 66A, 991-
13. V. RANDLE: *Mater. Sci. Tech*., 1999, 15, 246-252.
14. D. M. SAYLOR, A. MORAWIEC AND G. S. ROHRER: *Acta Mater.*, 2003, 51, 3675-3686
15. D. M. SAYLOR, B. S. EL-DASHER, T. SANO AND G. S. ROHRER: *J. Amer. Ceram. Soc.*, 2004, 87, 670-676.
16. D. M. SAYLOR, B. S. EL DASHER, A.D. ROLLETT AND G.S. ROHRER: *Acta Mater*., 2004, 52, 3649-3655.
17. K. L. MERKLE AND D. WOLF: *Philos. Mag*., 1992, 65A, 513-
18. W. B. HUTCHINSON, L. RYDE, P. S. BATE AND B. BACROIX: *Scripta Mater*. 1996, 35, 579-582.
19. I. CROSS AND V. RANDLE: *Scripta Mater*., 2003, 48, 1587-1591.

Acknowledgements

The work at Carnegie Mellon University was supported primarily by the MRSEC program of the National Science Foundation under Award Number DMR-0079996. The work at Swansea was partially supported by the Engineering and Physical Sciences Research Council.

Table 1 – Proportions of Σ boundaries and low angle boundaries in grain boundary engineered brass specimens

	% by length	% by number
Σ3	57.7	38.2
Σ9	3.4	6.7
Σ27	1.9	3.9
Σ81	1.1	2.3
Σ243	0.1	0.6
Low angle	2.6	2.9

Table 2 - Disorientations associated with misorientation angle/axis pairs on <110> in angle increments of 5° from 65° to 120°

Misorientation angle on <110> (º)	Equivalent disorientation (angle º/axis)
65	60.2/0.653 0.535 0.535
70	60/111
75	60.2/0.608 0.608 0.512
80	60.6/0.636 0.636 0.436
85	61.6/0.660 0.660 0.359
90	62.8/0.679 0.679 0.280
95	61.6/0.660 0.660 0.359
100	60.6/0.636 0.636 0.436
105	60.2/0.607 0.607 0.512
110	59.9/0.585 0.574 0.574
115	60.2/0.653 0.535 0.535
120	60/110

Table 3 – Examples of solutions for disorientations and equivalent misorientations with near-<111> axes.

Angle/axis (in nearest Miller indices) for disorientation	Angle/axis (in direction cosines) for disorientation	Angle/axis (in nearest Miller indices) for equivalent misorientation on <111>	Angle/axis (in direction cosines) for equivalent misorientation on <111>	Angular deviation from <111>
36º/322	39.9º/0.671 0.599 0.437	155º/111	159.4º/0.622 0.566 0.541	3.4º
21º/221	18.1º/0.691 0.687 0.226	100º/111	103.4º/0.607 0.606 0.514	4.3º

Table 4 – Length proportions of 'potentially special' boundaries, i.e. those misoriented on <110> , those misoriented on <111>, and low angle boundaries (see text for details).

Category	Proportion (%)
<111> axis (disorientation)	59.1
<110> axis (disorientation)	7.7
<111> axis (equivalent misorientation)	4.0
<110> axis (equivalent misorientation)	5.2
Low angle boundaries	2.6
Total	78.6

Figure captions

Figure 1. Orientation map from GBE brass showing $\Sigma 3^n$ boundaries up to n = 5, i.e. $\Sigma 243$. $\Sigma 3$, $\Sigma 9$, $\Sigma 27$, $\Sigma 81$ and $\Sigma 243$ are coloured red, blue, yellow, green and purple respectively. Low angle boundaries (3º-15º) are grey and all remaining boundaries are black.

Figure 2. Distribution of grain boundary planes, in multiples of a random distribution (MRD), for the <110> misorientation axis, segmented into misorientation angle bins of 10°. $\Sigma 3$s have been excluded.

Figure 3. Distribution of grain boundary planes, in multiples of a random distribution (MRD), for the <110> misorientation axis, segmented into misorientation angle bins of 10°. $\Sigma 3$s have been excluded.

Figure 4. Distribution of grain boundary planes, in multiples of a random distribution (MRD), for $\Sigma 27$b.

Figure 5. Orientation map in Fig. 1 showing (a) all grain boundaries in Table 4 in light grey and remaining boundaries in black (b) all boundaries in black.

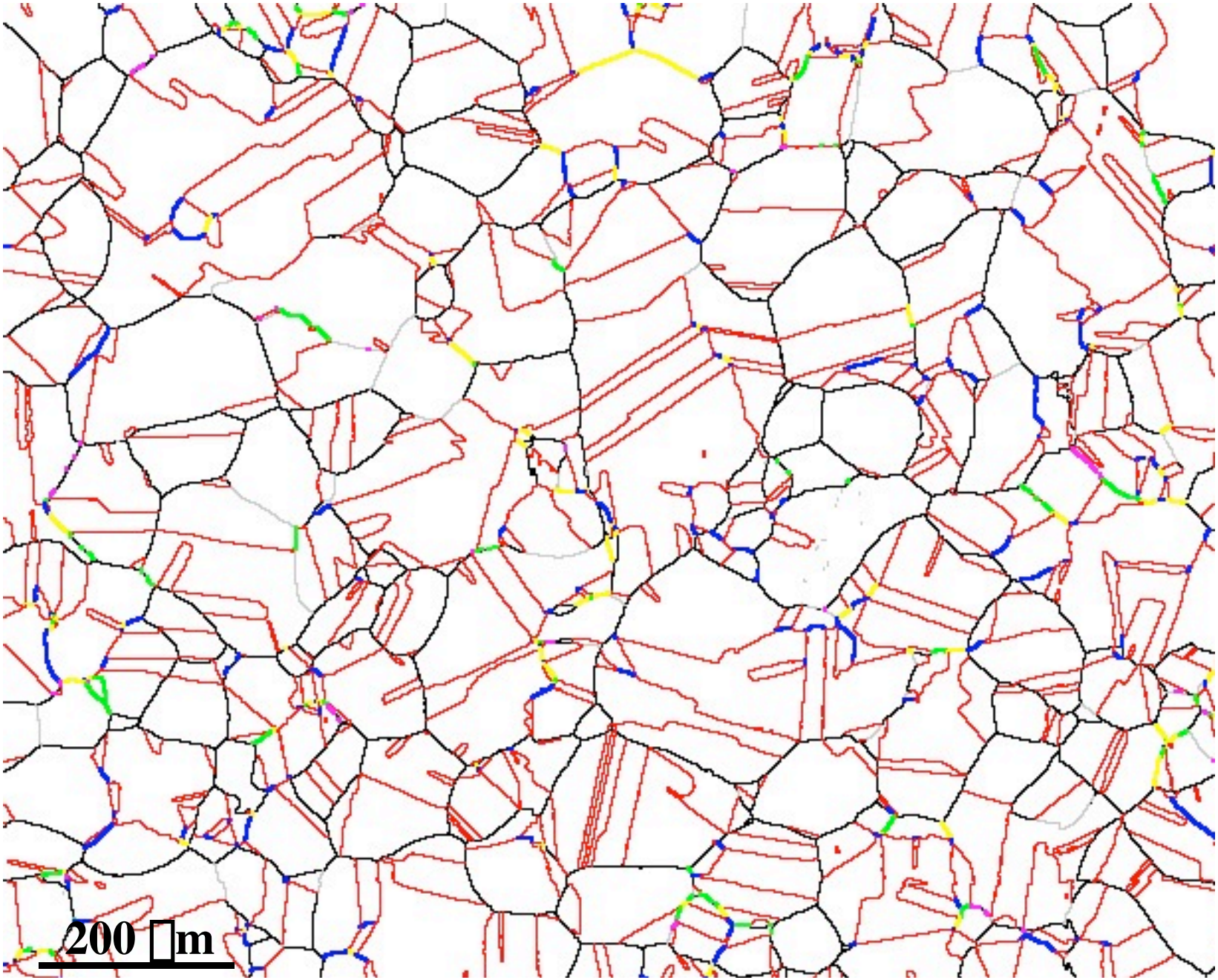

Figure 1

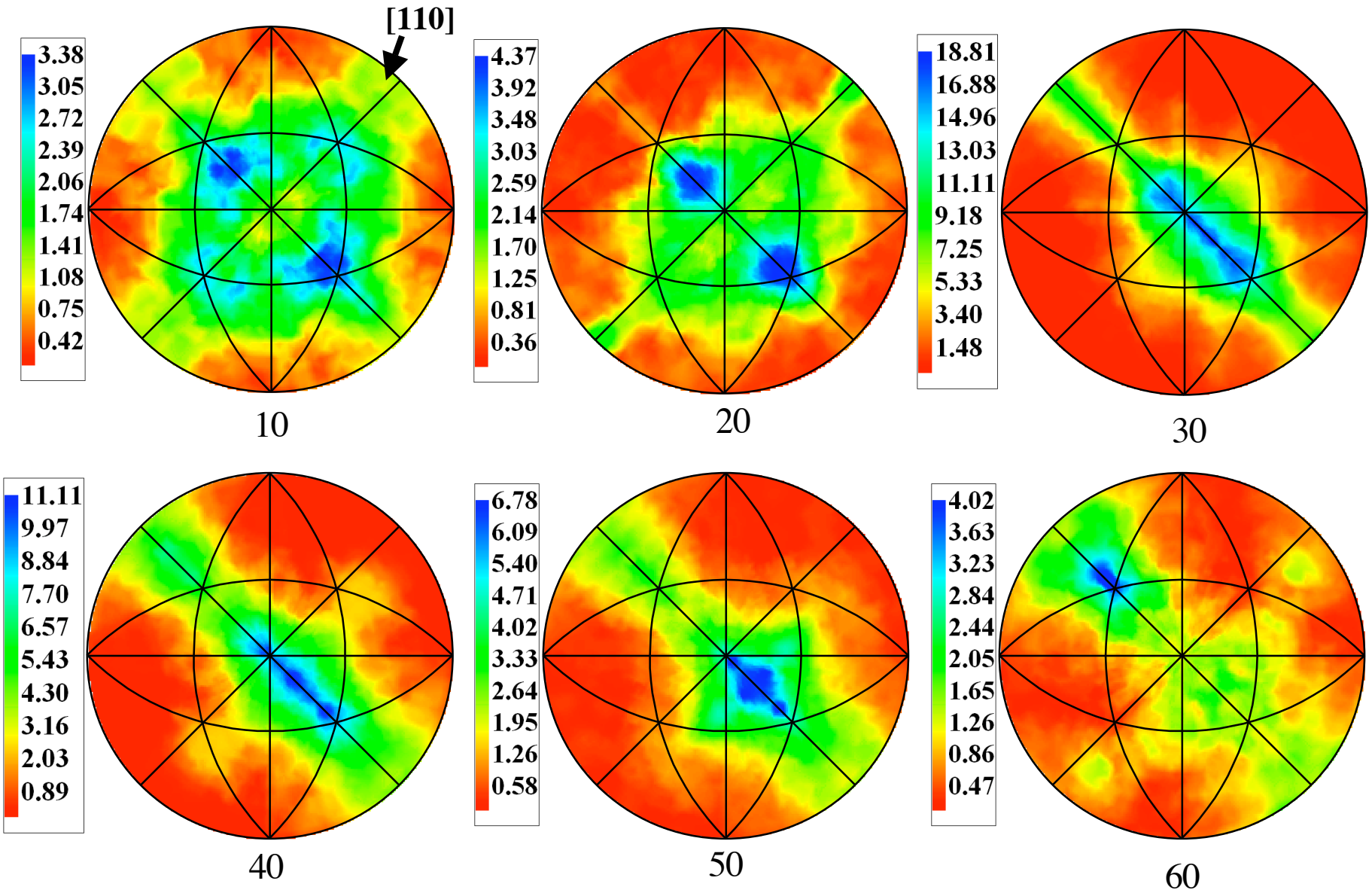
[110]
3.38
3.05
2.72
2.39
2.06
1.74
1.41
1.08
0.75
0.42
10
4.37
3.92
3.48
3.03
2.59
2.14
1.70
1.25
0.81
0.36
20
18.81
16.88
14.96
13.03
11.11
9.18
7.25
5.33
3.40
1.48
30
11.11
9.97
8.84
7.70
6.57
5.43
4.30
3.16
2.03
0.89
40
6.78
6.09
5.40
4.71
4.02
3.33
2.64
1.95
1.26
0.58
50
4.02
3.63
3.23
2.84
2.44
2.05
1.65
1.26
0.86
0.47
60

Figure 2

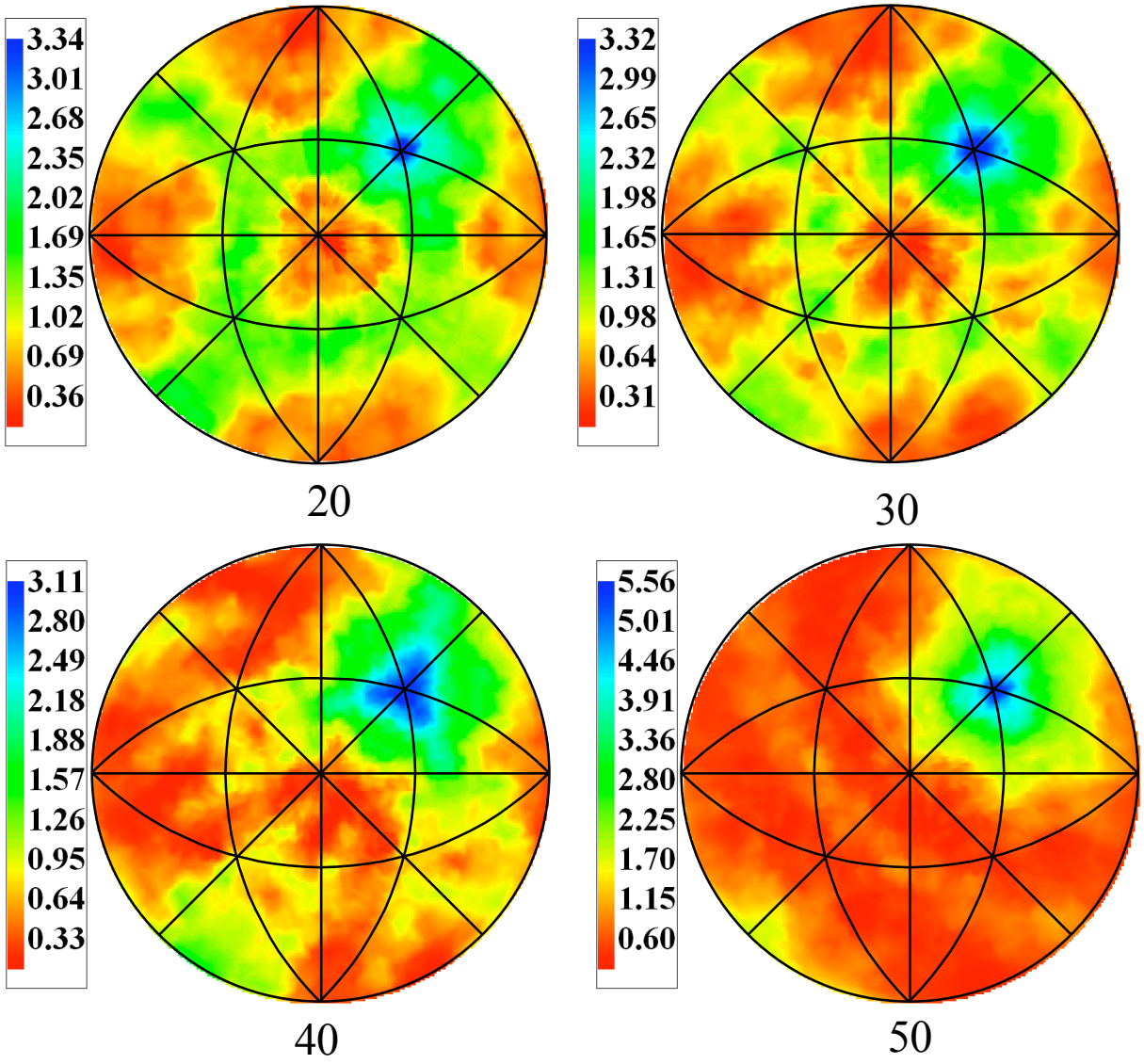
3.34
3.01
2.68
2.35
2.02
1.69
1.35
1.02
0.69
0.36
20
3.32
2.99
2.65
2.32
1.98
1.65
1.31
0.98
0.64
0.31
30
3.11
2.80
2.49
2.18
1.88
1.57
1.26
0.95
0.64
0.33
40
5.56
5.01
4.46
3.91
3.36
2.80
2.25
1.70
1.15
0.60
50

Figure 3

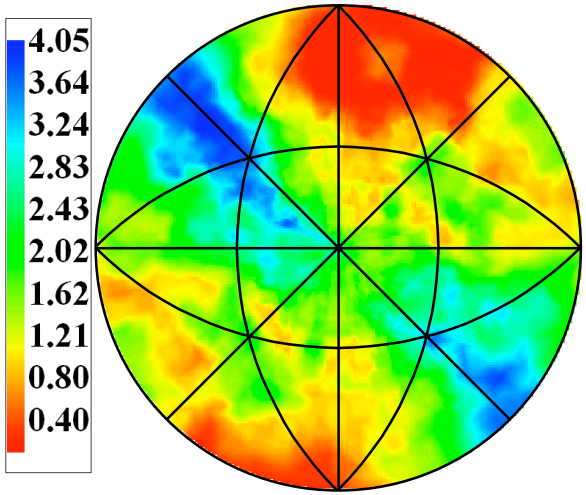

Figure 4

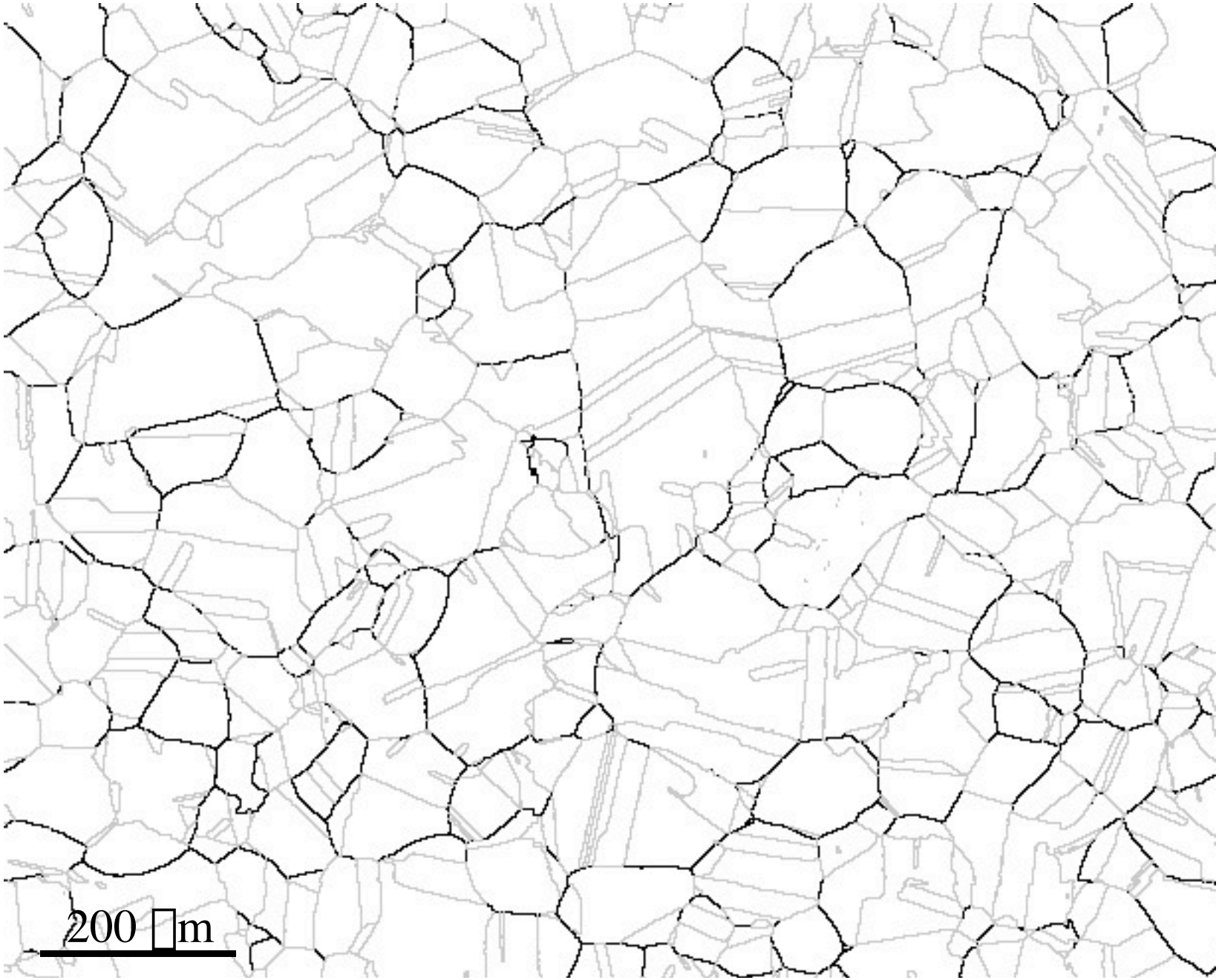

Figure 5a

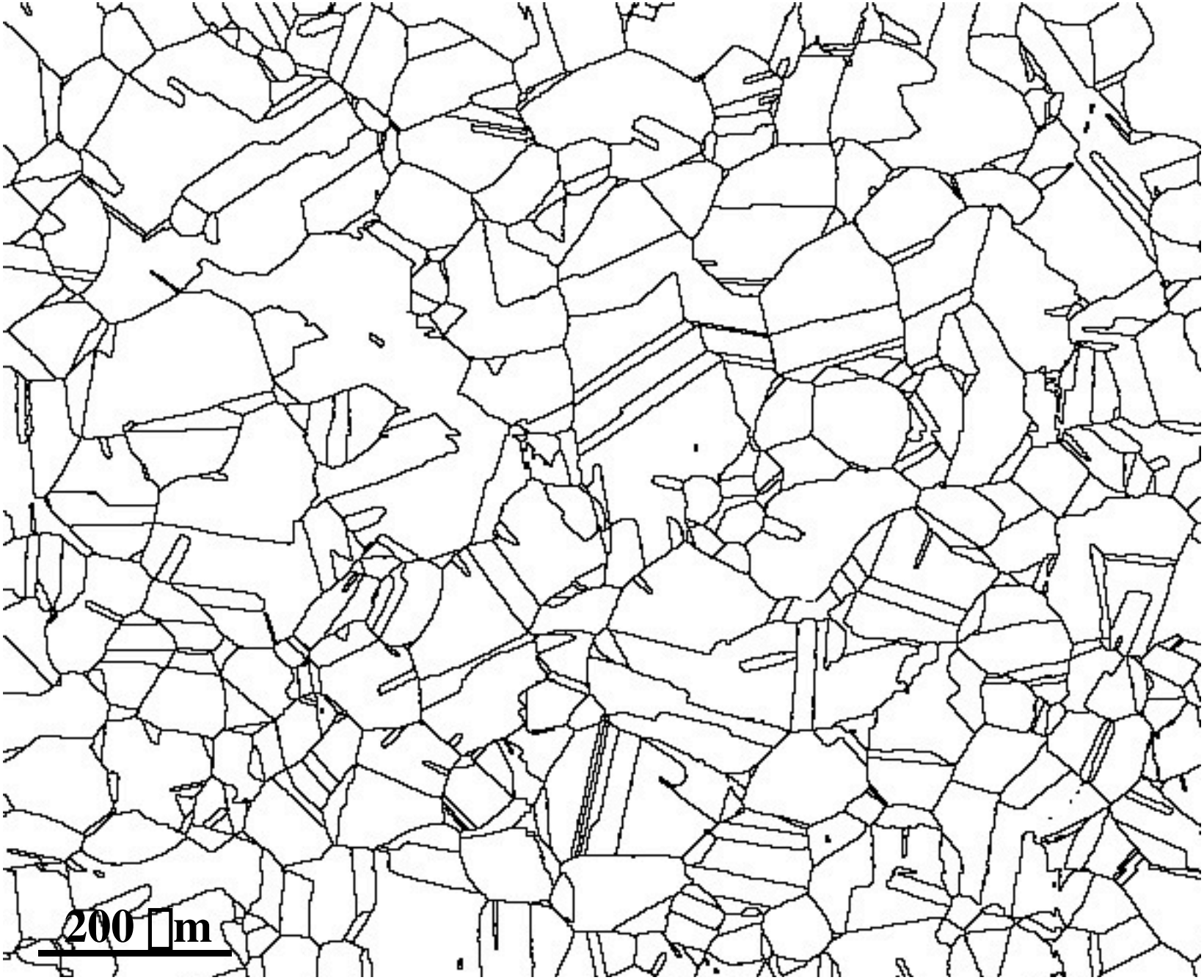

Figure 5b